ACADEMIC PRESS

Available online at www.sciencedirect.com
SCIENCE DIRECT®

Journal of Catalysis 217 (2003) 324–333

JOURNAL OF CATALYSIS

www.elsevier.com/locate/jcat

The nature and binding strength of carbon adspecies formed during the equilibrium dissociative adsorption of CH_4 on Ni–YSZ cermet catalysts

Nikolaos C. Triantafyllopoulos [a,b] and Stylianos G. Neophytides [a,*]

[a] *Foundation of Research and Technology Hellas, Institute of Chemical Engineering & High Temperature Processes, PO Box 1414, GR-26504 Rion Achaias, Greece*

[b] *Department of Chemical Engineering, University of Patras, PO Box 1414, GR-26500 Patras, Greece*

Received 2 October 2002; revised 3 February 2003; accepted 10 February 2003

Abstract

The equilibrium dissociative adsorption of CH_4 was studied over Ni–YSZ cermet catalysts for a deeper insight regarding the nature and binding strength of generated carbon species on the Ni–YSZ surface. Three main carbon species were detected by the reaction of carbon adspecies with H_2 to produce CH_4 or with O_2 to produce CO and CO_2. Carbidic species (C_c) are reactive with H_2 and O_2 at temperatures below 600 K while adsorbed carbon (C_a) species in equilibrium with CH_x species react with H_2 and O_2 above 600 K. Graphitic carbon layers (C_g) are formed upon CH_4 adsorption above 700 K and its main characteristic is the absence of any reactivity with H_2, to form CH_4. The binding energy of C_a species with respect to graphite decreases with increasing coverage ranging between 7.32 ± 0.03 and 6.5 ± 0.04 eV for the low (< 0.2 ML) and high (≈ 1 ML) coverage, respectively. The presence of 1% wt of Mo either suppresses the formation of adsorbed graphitic layers which are not reactive with H_2 or enhances the reactivity of adsorbed hydrogen atoms toward CH_4 at temperatures higher than 800 K, thus revealing the positive effect of Mo in inhibiting the formation of adsorbed graphitic layers.

Keywords: Carbon deposition; Ni–YSZ; Ni/Mo–YSZ; SOFC; CH_4 dissociation

1. Introduction

CH_4 is considered as the main energy source for fuel cell technology due to its large abundance and high H_2/C ratio as H_2 source. Solid oxide fuel cells (SOFCs) that operate at high temperature (1073–1173 K) can directly process steam reforming of CH_4 on the Ni/YSZ anode electrode [1–4] into CO, CO_2, and H_2, while CO and H_2 can be readily oxidized electrochemically at the three phase boundaries (Ni|YSZ|gas), generating electricity.

The aforementioned process termed as internal steam reforming of methane exhibits two serious problems: (i) the endothermic steam reforming reaction can cause a significant cooling effect with the development of large temperature gradients at the SOFC's entrance while (ii) the high $H_2O/CH_4 > 2$ ratio, which is necessary so that coke formation is avoided, results in the severe decrease of the fuel cell open-circuit potential (emf) and consequently its efficiency toward energy production.

An alternative utilization of CH_4 that recently received increasing attention is its direct electrochemical oxidation for the production of synthesis gas and electricity [5,6]:

$$CH_4 + O^{2-} \rightarrow CO + 2H_2 + 2e^-. \quad (1)$$

The reaction (1) is a very attractive process for SOFC applications, as we can combine in a single process the concepts of electricity production and useful chemical cogeneration (synthesis gas production). Synthesis gas can then be used for the production of various chemicals like methanol or for the oxo-synthesis and Fischer–Tropsch synthesis. Though reaction (1) is exothermic with relatively high emf (1.3 V at 1173 K) its main drawback from the catalytic and electrocatalytic point of view is the coke formation, which results in the rapid degradation of the anode. Carbon deposition takes place through the catalytic dissociative adsorption of CH_4 on the anode electrode surface [7–10]:

$$CH_4 \rightarrow C_{gr} + 2H_2. \quad (2)$$

Coking is considered one of the main causes of catalyst deactivation in catalytic reactions involving hydrocarbon transformation. However, it is already well established that

* Corresponding author.
E-mail address: neoph@iceht.forth.gr (S.G. Neophytides).

0021-9517/03/$ – see front matter
doi:10.1016/S0021-9517(03)00062-9

surface carbon adspecies leading to coke formation can also be the main reaction intermediates in several catalytic processes like CO hydrogenation [11–14], CH_4 reforming reactions [15], and CH_4 partial oxidation for the production of synthesis gas [16,17]. Considering that coke formation can be the main cause of serious operational problems the development of catalytic systems that are resistive to coke formation is becoming a major challenge. For this a vast literature both experimental [7–9,18–24] and theoretical [12, 13,25–29] was devoted to obtain a deeper insight of the surface chemistry of methane dissociative adsorption on various metals and the nature of the various carbon adspecies formed on the catalytic surface.

In order to investigate the possibility of the direct introduction of CH_4 into a SOFC the dissociative adsorption of CH_4 and the nature of the various carbon adspecies on Ni–YSZ and Ni/Mo–YSZ were studied by means of thermodynamic equilibrium measurements and temperature programming. The few studies, dealing with the catalytic properties of the Ni/Mo-supported catalysts on coke formation during steam reforming of hydrocarbons, show the positive effect of small Mo quantities on the reduction of the rate of carbon deposition on the Ni/Mo surface [30–34].

2. Experimental

2.1. Ni–YSZ and Ni/Mo–YSZ preparation and characterization

Ni–YSZ was prepared by the sol–gel method, which is described below. Zirconium tetra-*n*-butoxide was dissolved in 2-propanol and 1 N nitric acid diluted with the solvent. The final alkoxide concentration was 0.05 M and the water to alkoxide ratio was fixed at 3. The hydrolysis and condensation were carried out at room temperature under stirring for 2 days. In order to replace the dispersion medium of 2-propanol with water, excess water was added and 2-propanol was removed by evaporation. Yttrium nitrate hexahydrate and nickel nitrate hexahydrate were dissolved in 10 ml of water each and they were added to the sol and stirred for 1 day. The yttrium concentration was adjusted so that the content of Y_2O_3 is 8% mol in YSZ, while Ni was 50% wt. The sol obtained was dried and fired in 20% O_2/He mixture (20 cc STP/min) at 1123 K with a rate of 20 K/min. The Ni/Mo–YSZ bimetallic catalyst was prepared in the same way as that for NiO–YSZ. The sol was dried and fired at 573 K. Finally, Mo was added by wet impregnation, using MoO_3 diluted in a solution of NH_3, to obtain 1% wt Mo/Ni which was thereafter dried and calcined in 20% O_2/He mixture (20 cc STP/min) at 1123 K with a rate of 20 K/min.

BET and Ni surface areas were measured by the use of a QuantaChrome Autosorb-1 BET and chemisorption system, while XPS analysis was carried in an UHV equipped with a hemispherical analyzer (SPECS LH-10) and a twin-anode X-ray gun. For the in situ measurement of Ni CO uptake

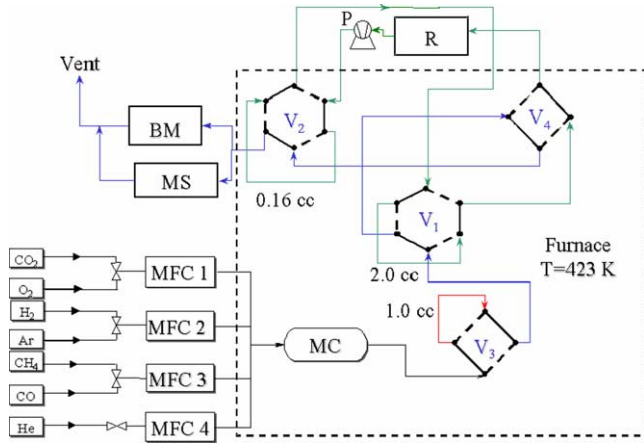

Fig. 1. Flow chart of experimental setup. **R**, reactor; **P**, recirculation pump; **V1–V4**, chromatographic valves; **MFC**, mass flow controllers; **MC**, mixing chamber; **MS**, quadrupole mass spectrometer; **BM**, bubble flow meter.

was carried out by injecting calibrated CO pulses through the catalyst bed by means of a sample loop (1 cc, V_3) (Fig. 1). He served as the carrier gas (30 cc STP/min), while CO mole fraction was monitored by the mass spectrometer. CO was injected several times until no significant difference could be seen in the areas of CO peaks eluted. By comparing the amount of CO detected by mass spectrometer and the amount of CO injected into the system, the quantity of CO adsorbed on the catalysts could be determined.

Ni particle size was measured by XRD (Philips PW18). The calculation was based on the X-ray line broadening of the diffraction peak according to Scherrer's equation [35]. Temperature-programmed reduction (TPR) profiles of the two catalysts were obtained by heating the samples from 300 to 1123 K at a rate of 20 K/min in 6% H_2/He mixture with a flow rate of 85 cc STP/min.

2.2. Experimental procedure

Thermodynamic studies were carried out in a closed reactor loop **R** (Fig. 1). A KNF Neuberger diaphragm pump **P** was used for the circulation of the gas inside the closed loop so that good mixing and uniform gas phase composition could be reached inside the reactor loop. The temperature of the experiments was varied between 573 and 873 K. The catalyst loading in the quartz tube reactor was 300 mg while the initial amount of the reactants (CH_4 or CO) injected into the reactor loop varied between 6 and 14 μmol so that the amount of carbon formed on the surface would vary from low coverage (0.05 monolayers) up to 2 monolayers (ML). The reactor outlet was monitored by a Balzers Omnistar quadrupole mass spectrometer. The experimental procedure for both reactions is as follows:

(i) The catalytic bed was heated to 1123 K with a rate of 20 K/min under a flow of 2% H_2/He mixture (122 cc STP/min). Then the reactor was purged with pure He for 30 min. Subsequently the reactor was cooled to the

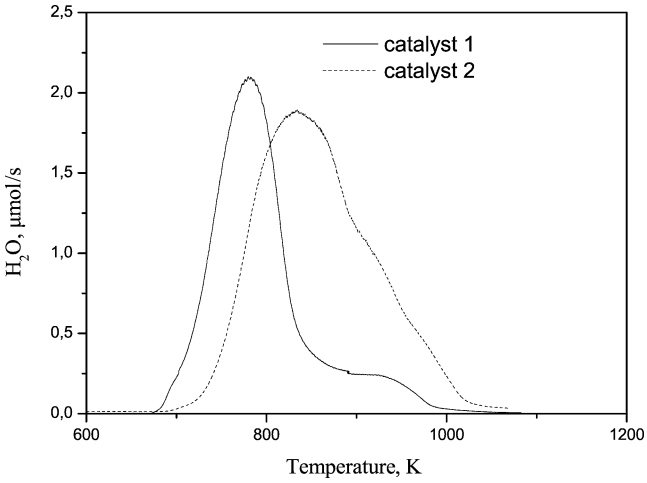

Fig. 2. Temperature-programmed reduction of NiO–YSZ (catalyst 1) and Mo/NiO–YSZ (catalyst 2) in 5.2% H_2/He. Total molar flow rate, 73 μmol/s; ramp rate, 20°/min.

reaction temperature (under closed loop conditions), and the feed gas was set up through the loop by the 6-port valve **V1** (Fig. 1) for the injection of a specific amount of CO or CH_4 into the reactor loop.

(ii) After the injection, the system was left for a time period of 30 min to reach equilibrium. The equilibrium was monitored by withdrawal of 0.16 cc aliquots from the reactor loop through the chromatographic valve **V2** (Fig. 1), which were analyzed by the mass spectrometer.

(iii) Thereafter the reactor loop was purged with He flow (30 cc STP/min) by means of valve V_4 and the catalytic bed was rapidly cooled at room temperature. The carbon species formed on the catalytic surface were removed by temperature-programmed surface reaction (TPSR) under H_2/He flow or by temperature-programmed oxidation (TPO) of the surface carbon by introducing pulses of O_2 at low temperature. These two procedures are described in detail below.

2.2.1. TPSR with H_2

After the reactor was cooled at room temperature the He stream, flowing through the reactor in step (iii), was replaced by 2% H_2/He (152 cc STP/min) and the Ni–YSZ bed was heated from 300 to 1123 K at a ramp rate of 20 K/min. The amount of methane produced was recorded as a function of temperature by the mass spectrometer.

2.2.2. Oxidation of surface carbon with O_2

Following step (iii) the reactor loop was purged with He and simultaneously cooled to 473 K. A quantity of 6 μmol of O_2 was injected into the catalytic bed by means of the 4-port valve **V3** (Fig. 2) and subsequently the reactor was cooled to room temperature. The whole amount of O_2 was adsorbed on the catalyst surface. Thereafter the reactor was purged with He and was linearly heated with a ramp rate of 20 K/min to 1123 K while CO, CO_2, and H_2 produced were recorded by the mass spectrometer.

Steps (i)–(iii) of the experimental procedure were repeated by varying each time the initial amount of CH_4 injected into the reactor or/and the temperature of the catalytic bed.

3. Results

Table 1 shows the physical properties of catalysts 1 and 2 regarding their surface area, Ni particle size, and composition. Ni surface area that was measured as total H_2 uptake was always larger than that measured by CO chemisorption in situ. This might be due to CO dissociative adsorption into adsorbed O and C species while O species are rendering part of the Ni surface inactive to CO chemisorption. The XRD spectrum of the reduced sample shows very clearly the formation of YSZ and Ni phases while the mean particle size of Ni was calculated as 19.03 and 33 nm for catalysts 1 and 2, respectively (Table 1). However, it is somewhat risky to attribute the observed difference in particle size and Ni surface area only to the existence of Mo since more measurements and larger number of samples (even following different preparation methods) are needed so that we can reach safe conclusions. XRD measurements of the fresh and used samples did not show any significant changes in Ni particle size. Ni, Zr, Y, and Mo content in the Ni–YSZ and Ni/Mo–YSZ samples was estimated by means of XPS analysis and is shown in Table 1. It is worth noting that Mo was hardly detectable by XPS because of its low quantity, its dilution in the bulk of Ni, and the enrichment of the surface with Ni [36]. As indicated in Ref. [36], where the compilation of surface segregation energies of all transition metals in all transition metals is estimated, Ni strongly segregates on the surface of the Mo/Ni alloys. Fig. 2 shows TPR spectra of catalysts 1 and 2. For both samples the maximum of the reduction peak is located above 750 K. The Mo-containing sample (catalyst 2) is reduced with greater difficulty than

Table 1
Physical properties Ni–YSZ catalysts

	S_{BET}	H_2 uptake	CO uptake	Ni crystal size	Nominal composition (% wt)					XPS (% wt)			
	(m^2/g)	(μmol/g)	(μmol/g)	(nm)	Ni	Zr	Y	O	Mo[a]	Ni	Zr	Y	O
Catalyst 1	11.6	29.3	10	19.06	50	31.9	5.4	12.7	–	34.7	33.1	6.6	25.7
Catalyst 2	4.1	16.6	9	33.5	49	31.9	5.4	12.7	1	50.1	20.7	6	20

[a] Mo was hardly detectable by XPS.

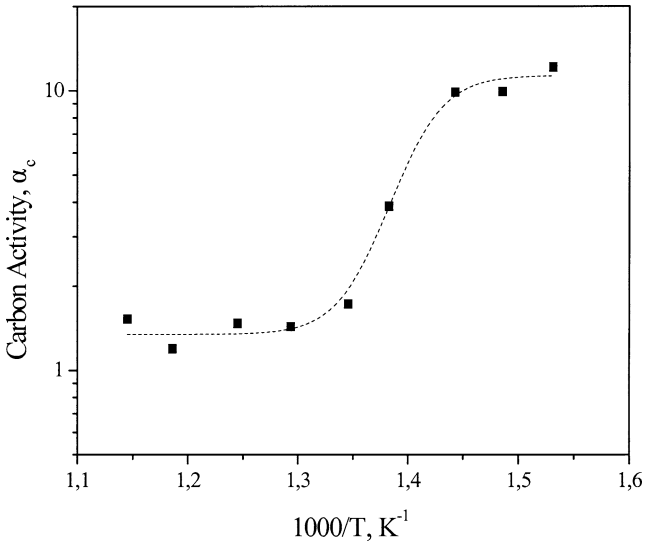

Fig. 3. Carbon activity, α_c, during CH_4 equilibrium dissociative adsorption. $n_{CH_4} = 14$ μmol. Catalyst 1.

catalyst 1, exhibiting peak maximum at 835 K, i.e., 35 K higher than catalyst 1, while the water peak is broader than the major peak observed for catalyst 1. The reduction temperatures of the two samples correlate satisfactorily with reported values in the literature for Ni–YSZ cermet [9].

Thermodynamic equilibrium experiments of CH_4 dissociative adsorption were curried out at carbon coverages ranging between fractions of a monolayer and up to 2 monolayers. These equilibrium experiments can be used for the estimation of the binding energy of the various carbon adspecies formed during the dissociative adsorption of methane on the Ni surface. Fig. 3 shows the dependence of carbon activity on temperature when a dose of 14 μmol of CH_4 is introduced into the reactor loop. Temperature varies from 570 to 870 K. The activity of carbon formed is given by

$$\alpha_c = \frac{K_{CH_4}}{P_{H_2}^2 / P_{CH_4}}, \tag{3}$$

where K_{CH_4} is the equilibrium constant of reaction (2) and P is the measured equilibrium partial pressures of H_2 and CH_4. It is quite interesting to note, in Fig. 3, the sharp decrease in the activity of carbon (α_c) at temperatures around 700 K. It can be seen that α_c at temperatures higher than 700 K is approaching 1, which corresponds to the activity of graphitic carbon.

In order to elucidate the nature of the carbon adspecies, formed on the catalytic surface during CH_4 equilibrium dissociative adsorption, temperature-programmed surface reaction experiments were carried out under H_2 flow through the catalytic bed of Ni/YSZ. H_2 reacts with the adsorbed carbon species forming CH_4. This is shown in Fig. 4 where the rates of formation of CH_4 are plotted versus temperature. The different TPSR spectra correspond to various carbon deposition equilibrium experiments, which

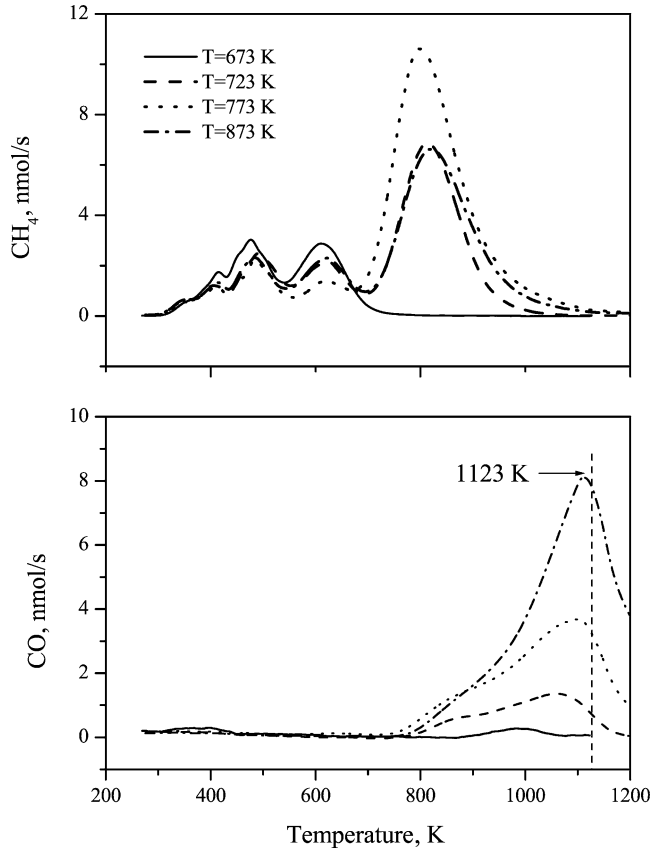

Fig. 4. Temperature-programmed surface reaction (TPSR) of surface carbon under 2.8% H_2/He flow, deposited during equilibrium dissociative adsorption of CH_4. Total molar flow rate, 134 μmol/s. Ramp rate, 20°/min, $n_{CH_4} = 14$ μmol. Catalyst 1.

were carried out at different temperatures. It can easily be concluded that the TPSR spectra of Fig. 4 can be divided into the low temperature (below 700 K) and high temperature (above 700 K) regions. The low temperature region consists of at least three CH_4 peaks and it ranges between 350 and 700 K while these carbon/carbonaceous (hereafter referred to as C_c) species, which are reactive at low temperatures, are formed in the whole temperature range that equilibrium experiments were carried out. The high temperature peak consists of one CH_4 peak, which exhibits a maximum at 810 K and corresponds to carbon species (hereafter referred to as C_a) that have been formed during CH_4 dissociation at temperatures above 670 K. Another very interesting feature of the TPSR experiments is the rather unexpected formation of CO, which is detected at temperatures above 800 K. This unexpected CO formation under H_2 flow can be attributed to the oxidation of these H_2 nonreactive carbon species (hereafter referred to as C_g), by reactive oxygen species of YSZ that can be evolved at temperatures above 850 K [37,38]. Fig. 5 shows the effect of temperature, at which the equilibrium experiments were carried out, on the total carbon quantity deposited and on the distribution of the CH_4 and CO produced during the TPSR experiment. CH_4 quantity exhibits a maximum

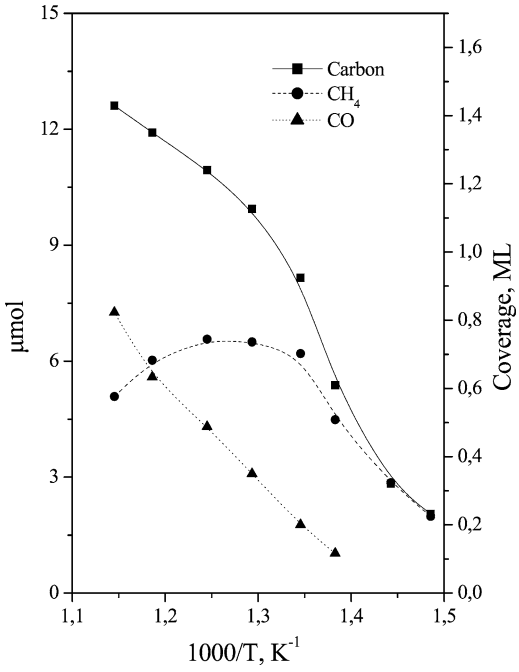

Fig. 5. Effect of temperature on the deposited quantity of the various carbon species deposited during the equilibrium dissociative adsorption of CH_4. Conditions as in Fig. 4. Catalyst 1.

around 750 K while CO quantity increases monotonously with increasing temperature. It is also worth noting that C_g species are observed when carbon adspecies, corresponding to the high temperature CH_4 peak (C_a), is developed on the Ni surface (Fig. 4).

In order to study the effect of H_2 partial pressure on the formation of the various carbons species different H_2/CH_4 ratios were introduced into the reactor, while CH_4 quantity was kept constant at 14 μmol. The TPSR spectra of Fig. 6 depict the effect of the H_2/CH_4 ratio that was introduced into the reactor loop, on the distribution of the various carbon adspecies on the Ni–YSZ surface, during the equilibrium dissociative adsorption of CH_4. It is very clearly shown that upon increasing H_2 partial pressure C_a species coverage decreases and disappears at $H_2/CH_4 = 1$, while a slight increase in the C_c species coverage is observed. The quantity of the C_g species does not vary significantly with increasing H_2/CH_4 ratio (Fig. 6). However at $H_2/CH_4 = 1$ they are not detected in the TPSR spectra similar to the case of C_a species. The activity of the carbon species formed during the H_2/CH_4 equilibrium experiments is calculated by Eq. (3) and it is plotted versus H_2/CH_4 ratio as shown in Fig. 7. Similar to the carbon activity shown in Fig. 3 a threefold increase in carbon activity (α_c) is observed, with increasing H_2/CH_4 ratio, which corresponds to the decrease in the coverage of C_a and C_g species.

A similar picture can be observed during the temperature-programmed oxidation of the adsorbed carbon/carbonaceous species on the Ni surface (Fig. 8). As can be observed the low temperature reactive adspecies (C_c) are oxidized almost completely into CO_2 while CO is formed with high

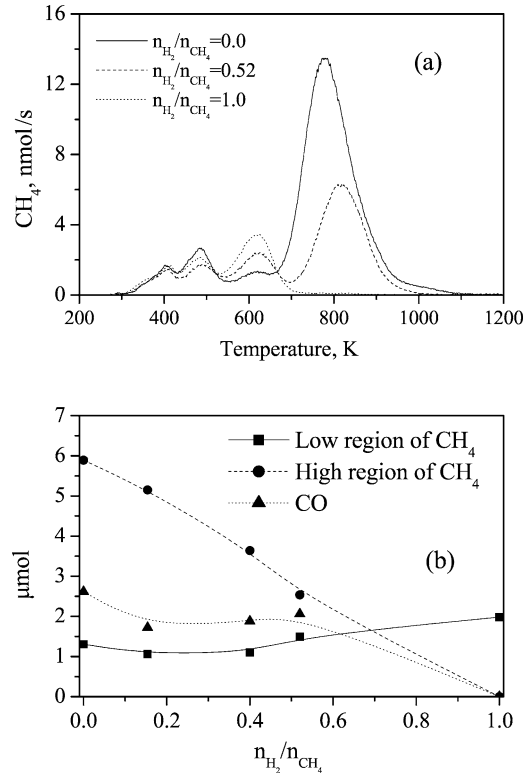

Fig. 6. TPSR spectra of surface carbon under 2.8% H_2/He flow (a) and distribution of C_c, C_a, and C_g species for various n_{H_2}/n_{CH_4} ratios (b), $n_{CH_4} = 14$ μmol. Total molar flow rate, 134 μmol/s; ramp rate, 20°/min. Catalyst 1.

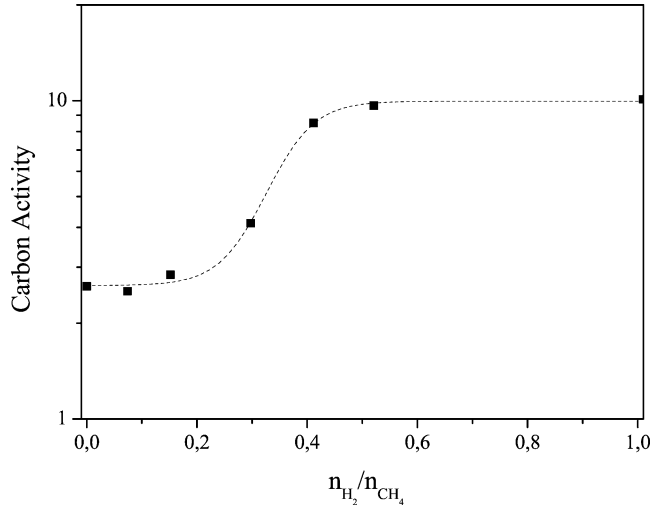

Fig. 7. Effect of the initial n_{H_2}/n_{CH_4} ratio on carbon activity α_c. Conditions as in Fig. 6. Catalyst 1.

selectivity by the oxidation of the high temperature region carbon species (C_a and C_g). It is worth noting that the low temperature oxidation peak, which corresponds to C_c species, is a single peak giving a single maximum at 600 K in contrast to the corresponding low temperature methanation peaks, which are distributed within a temperature range of 400 K (300–700 K). Another very significant observation is

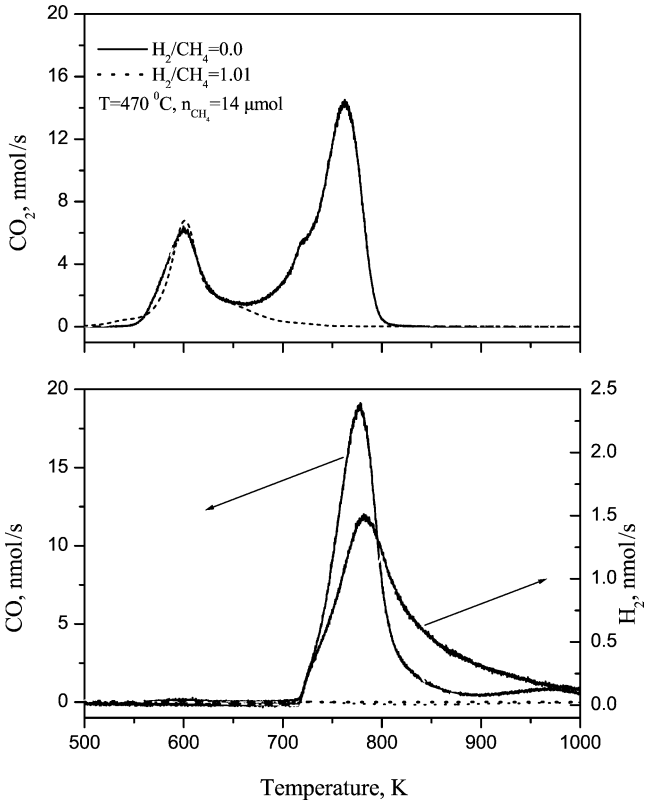

Fig. 8. Temperature-programmed oxidation (TPO) of surface carbon for different initial n_{H_2}/n_{CH_4} ratios, $n_{CH_4} = 14$ μmol. Adsorbed O_2 quantity at 470 K, 6 μmol. Ramp rate, 20°/min. He molar flow rate, 26 μmol/s. Catalyst 1.

the evolution of small amount of H_2 (< 5% of CO produced) that seems to coincide with the peak of CO evolved at around 780 K, thus indicating the existence of stable hydrogenated carbon species (CH_x). In fact H_2 evolution, instead of H_2O as the expected oxidation product, can be attributed to kinetic factors related to the limited amount of oxygen that was initially adsorbed on the Ni surface, i.e., before the TPO experiment. However, the TPO experiment of Fig. 8 shows that carbon is oxidized with higher selectivity compared to the oxidation of H_2.

Fig. 9 shows detailed equilibrium measurements that depict the effect of temperature on the equilibrium product for the dissociative adsorption of CH_4 toward the production of adsorbed carbon species and H_2 on catalysts 1 and 2. It must be noted that the behavior of catalyst 2 containing 1% wt Mo was similar to that of catalyst 1, regarding the type of generated carbon species on the surface during the equilibrium dissociative adsorption of CH_4. The difference was the absence of CO formation during TPSR experiments. Instead, carbon species formed in the equilibrium experiments at temperatures above 770 K (region III in Fig. 9) would produce CH_4 at elevated temperatures even above 900 K (Fig. 10). However, larger amounts of Mo exceeding 5% wt do affect significantly the nature of deposited carbon [39]. The solid line in Fig. 9 corresponds to the equilibrium of reaction (2) resulting in the formation of graphitic carbon and

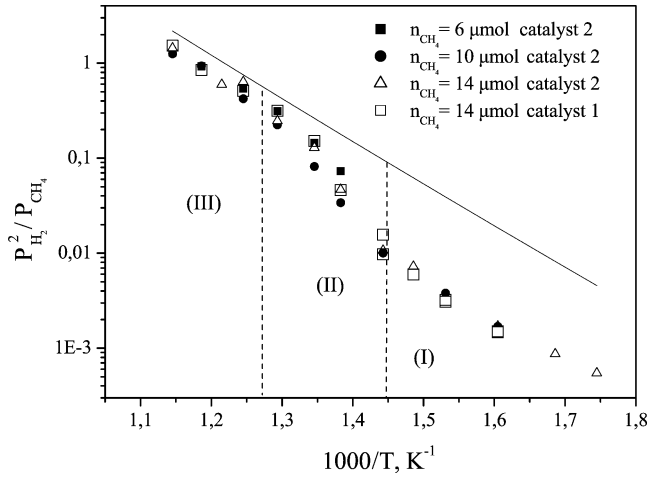

Fig. 9. Effect of temperature on the equilibrium product $P_{H_2}^2/P_{CH_4}$ of reaction (6) for various n_{CH_4} values. Solid line corresponds to the Van't Hoff diagram of reaction (6).

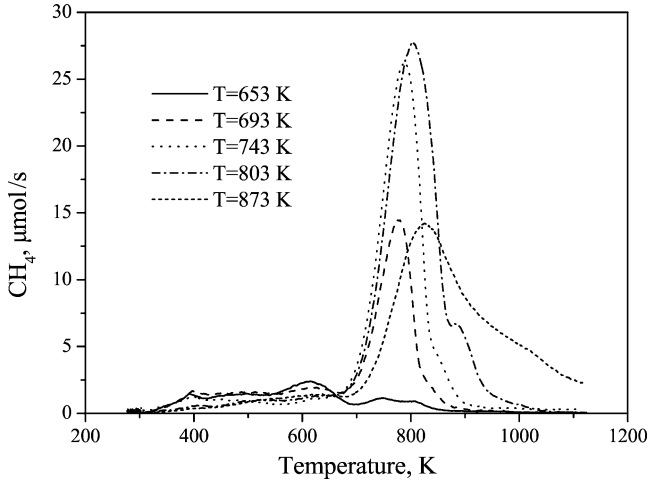

Fig. 10. TPSR of surface carbon under 2.8% H_2/He flow, deposited during equilibrium dissociative adsorption of CH_4. Total molar flow rate, 134 μmol/s. Ramp rate, 20°/min. $n_{CO} = 14$ μmol. Catalyst 2.

H_2. Fig. 9 shows the existence of three regions. The first one (labeled as I in Fig. 9) is the low temperature region corresponding to the formation of C_c species. The second region (labeled as II in Fig. 9) corresponds to the transition where the C_a species are developed until they reach to a maximum deposited amount, thus corresponding to the transition from high to low thermodynamic activity as depicted in Fig. 3. In the third region (labeled as III in Fig. 9) the equilibrium product is very close to the equilibrium of reaction (2) corresponding to graphite formation.

4. Discussion

The nature of various carbon species has received an increased interest by a vast number of researchers due to its dual role as intermediate species for hydrogenation reactions and as deactivation agent in its graphitic form. It

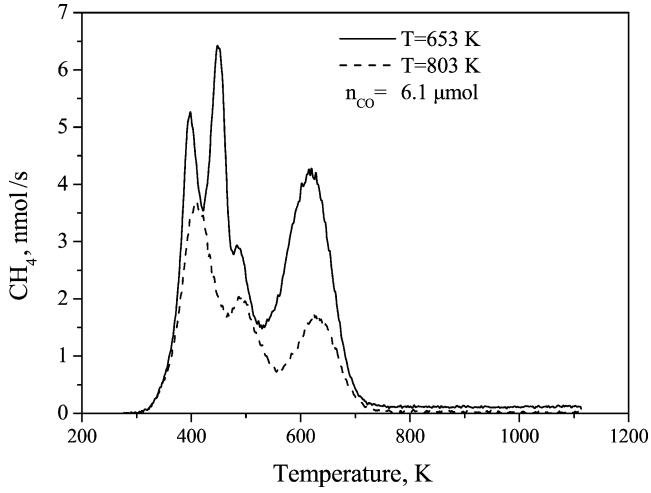

Fig. 11. TPSR of surface carbon under 2.1% H_2/He flow, deposited during equilibrium dissociative adsorption of CO. Total molar flow rate, 132 μmol/s. Ramp rate, 20°/min. $n_{CO} = 6$ μmol. Catalyst 1.

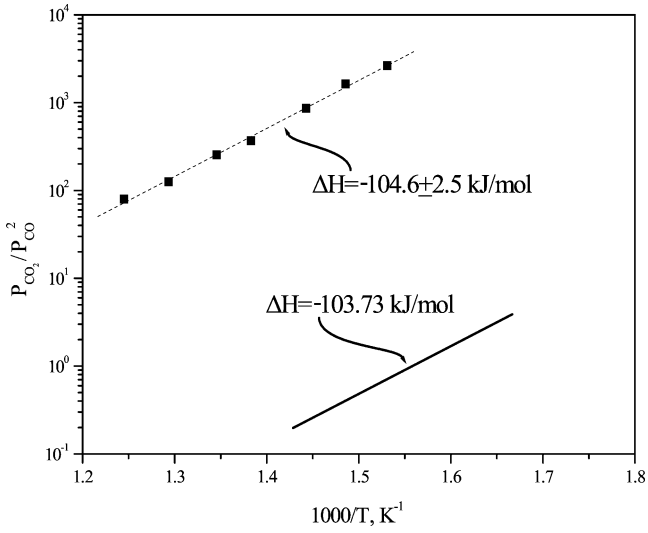

Fig. 12. Effect of temperature on the equilibrium product P_{CO_2}/P_{CO}^2 of reaction (4) (catalyst 2). Solid line corresponds to the Van't Hoff diagram of reaction (4).

has been already well established experimentally that the active carbon species leading to hydrogenated products are in the carbidic form while its graphitic form is considered inactive for hydrogenation reactions [14]. As already noted, in the present study, the equilibrium dissociative adsorption of CH_4 resulted in the formation of three types of species, as these were detected based on their reactivity with H_2 and O_2 to form CH_4 and carbon oxides.

4.1. Low temperature reactive carbon species (C_c)

The low temperature reactive carbon species labeled as C_c can be attributed to carbidic carbon bonded with the Ni surface. Similar equilibrium experiments, with CO dissociative adsorption on Ni–YSZ, resulted in adsorbed carbon deposits whose TPSR spectra under H_2 flow (Fig. 11) seem to be very similar to the corresponding low temperature region TPSR spectrum following the dissociative adsorption of CH_4 (Figs. 4 and 6a). The carbidic nature of the carbon species originating from the dissociative adsorption of CO is deduced by the calculated enthalpy change of the reaction ($\Delta H = -104.6 \pm 2.5$ kJ/mol) derived by the slope of the plot of the equilibrium product P_{CO_2}/P_{CO}^2 versus $1/T$ (Fig. 12). This enthalpy change corresponds to the reaction of CO with Ni for the production of Ni_3C and CO_2,

$$2CO + 3Ni \leftrightarrow CO_2 + Ni_3C, \quad (4)$$

thus being in excellent agreement with the calculated theoretical value which is equal to -103.73 kJ/mol at 700 K. The entropy change calculated from the data of Fig. 12 is equal to -94.7 ± 3.6 J/mol K, which is by 67.43 ± 3.6 J/mol K less than that corresponding to reaction (4). This rather indicates that the carbidic species formed during CO dissociative adsorption are surface species with a higher degree of freedom.

On the contrary as it is very clearly shown in the low temperature region I of Fig. 9 the calculated enthalpy change corresponding to the dissociative adsorption of CH_4 is equal to 97.8 ± 3.3 kJ/mol, thus indicating that under equilibrium conditions the generated carbon species do not react with Ni to form carbide. It is rather plausible to assume that the carbon species formed under equilibrium conditions is mainly composed of hydrogenated carbon (CH_x) ending in and being in equilibrium with a very small coverage of adsorbed carbon C_a on the Ni surface. The existence of CH_x species can also be deduced by the evolution of H_2 during the TPO experiments as depicted in Fig. 8. Alstrup and Tavares proposed kinetic expressions for the carbon formation on Ni and Ni–Cu supported on silica which take into account as a rate limiting step one of the successive dehydrogenation steps of CH_4 into CH_x species [7,8]. Upon opening the reactor loop and purging the reactor with He it is rational to consider that the hydrogenated carbon species are decomposed forming a carbidic layer, which is then hydrogenated into CH_4 at temperatures below 700 K, thus giving the characteristic TPSR spectra of Figs. 4, 6, and 10.

In a very comprehensive article Klinke et al. [25] carried out theoretical calculations on the binding energy of adsorbed carbon species at different coverages on Ni(111) surface. They concluded that at low coverages ca. 0.25 ML the binding energy of carbon adatoms with Ni(111) surface is 6.68 eV. Correspondingly the slope of the exponential fitting of region (I) (Fig. 9) can give an estimate of the binding energy of adsorbed carbon on the Ni–YSZ surface at these low coverages with respect to graphite [21]. Fig. 13 shows the total coverage of carbon species that corresponds to the experimental data of Fig. 9. The coverage of deposited carbon adspecies, in the low temperature region (I), is quite small (< 0.2) while it does not vary significantly with increasing temperature. In this respect the diagram of region (I) in Fig. 9 can be considered as the isostere for CH_4 dissociation on Ni–YSZ into adsorbed carbon species and H_2. According to

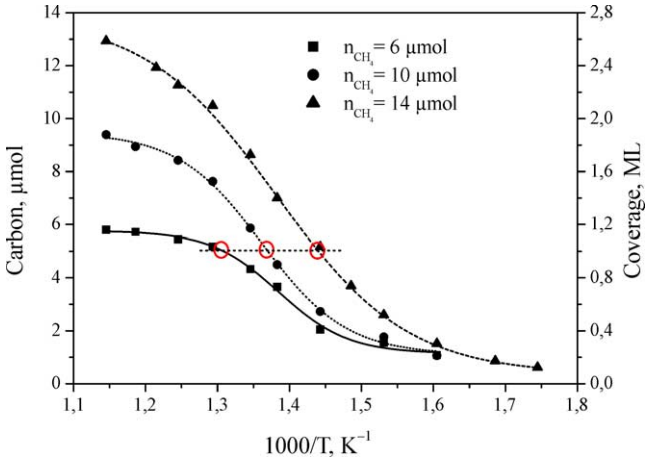

Fig. 13. Surface carbon coverage during CH_4 equilibrium dissociative adsorption for various initial amounts of CH_4. Conditions as in Fig. 9. Catalyst 2.

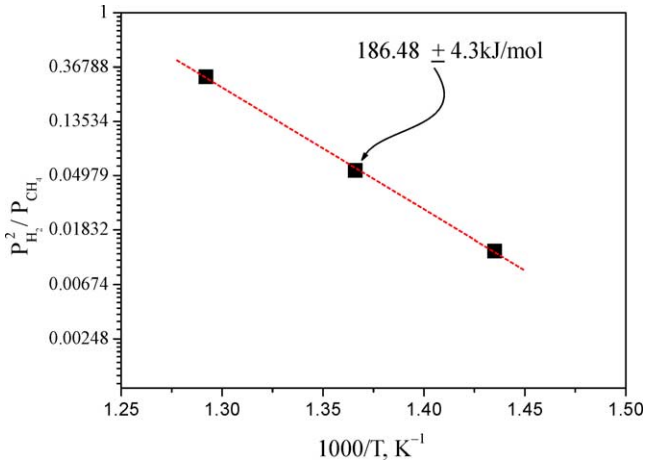

Fig. 14. Isostere for CH_4 equilibrium dissociative adsorption corresponding to carbon coverage of 1 ML based on the combination of data from Figs. 9 and 13. Catalyst 2.

the aforementioned considerations the binding energy of adsorbed carbon species on the Ni–YSZ surface, corresponding to the enthalpy change of 97.8 ± 3.3 kJ/mol as this was estimated from region I of Fig. 9, is equal to 7.32 ± 0.03 eV, rather close to the low coverage value of 6.68 eV that was calculated theoretically [25].

4.2. Adsorbed carbon at higher coverage (C_a)

As was shown in Fig. 4 C_a species appears at temperatures above 670 K while its coverage depends both on temperature and on P_{H_2}/P_{CH_4} ratio (Fig. 6). Further its appearance is accompanied by the decrease of adsorbed carbon species activity (α_c) so that it approaches unity at higher temperatures (Fig. 3), thus coming closer to the activity of graphitic carbon. However, the gradual decrease of the carbon species activity with increasing temperature and decreasing P_{H_2}/P_{CH_4} (Figs. 3 and 7), or similarly as shown in Fig. 9 the corresponding gradual approach of the equilibrium product $P_{H_2}^2/P_{CH_4}$ to that of reaction (2), denotes that the binding strength of C_a species with the Ni surface varies with increasing coverage. Combining the data of Figs. 9 and 13 we construct the isostere at constant carbon coverage (1 ML or ca 5 μmol carbon adsorbed) by plotting $P_{H_2}^2/P_{CH_4}$ versus $1/T$ (Fig. 14). The slope of the curve corresponds to the enthalpy of the reaction,

$$CH_4 \leftrightarrow C_a + 2H_2, \tag{5}$$

which is found to be equal to 186.48 ± 4.3 kJ/mol. The difference of the enthalpies of reactions (5) and (2) equals 101.48 ± 4.3 kJ/mol, thus corresponding to the enthalpy of formation of C_a species with respect to graphite. Accordingly its binding energy is 6.5 ± 0.04 eV. Therefore it can be concluded that the gradual increase of the C_a species coverage results in the weakening of the carbon bond with the Ni surface by ca 0.8 eV as compared to the low coverage binding energy of region I (Fig. 9). Further increase in temperature and carbon surface concentration most probably results in the formation of adsorbed graphitic layer (Fig. 9 region III).

Takeuchi and Wise [21] studied the thermodynamic properties of adsorbed carbon on Ni/Al_2O_3 catalysts originating from the dissociative adsorption of CO. They reported that the enthalpy of formation of adsorbed carbon species with respect to graphite decrease with increasing coverage ranging between 52 and 35 kJ/mol corresponding to coverages 0.5–0.9 ML. However, based on theoretical ab initio calculations, Klinke et al. [25] concluded that the binding energy of adsorbed carbon species on Ni(111) decreases with increasing coverage because of the development of direct carbon–carbon interactions on the surface. The binding energy of 1 ML of adsorbed carbon was estimated equal to 4.97 eV which is almost 2 eV less than the corresponding estimated value at 0.25 ML. Further increase of carbon concentration to 2 ML results in the formation of adsorbed graphite with binding energy 7.75 eV which corresponds mainly to carbon–carbon bonding. At this point it must mentioned that the present experimental conclusions are in very good qualitative agreement with the conclusions of Klinke et al. [25]. Beyond the inherent discrepancies due to the nature of the theoretical approximations, it must be noted that the use of a polycrystalline sample instead of a single crystal plane is also the main reason for the discrepancies between the present experimental results and the theory reported by Klinke et al.

4.3. Graphitic carbon layers (C_g)

As already presented in the TPSR spectra (Fig. 4) CO is evolved at temperatures above 800 K, though a 2% H_2/He mixture was flowing through the reactor. Two factors should coincide for the CO formation at these high temperatures: (i) the nonreactivity of these carbon species with H_2 to form

CH_4 and (ii) the existence of O_2 source to oxidize residual carbon.

It is already well established that graphitic carbon is not hydrogenated into CH_4 or any other hydrogenated species [14]. In his pioneering work Tibbetts developed a model, by means of the VLS (vapor-liquid-solid) theory, which shows that carbon precipitates into its tubular basal graphitic form because of the exceptionally low surface free energy of these graphitic planes, thus rendering graphitic carbon tubes chemically stable [40]. Baker and Metcalf [9] performed CH_4 adsorption experiments on Ni–YSZ cermet with 69.4% wt Ni. The hydrogenation of carbon species, which were formed by CH_4 adsorption at various temperatures, produced CH_4 with peak maxima at 730 and 940 K while the amount of carbon that was formed at adsorption temperatures above 900 K was significantly less reactive with H_2 to form CH_4 [9]. Thus, it is quite rational to consider that C_g species belong to graphitic layers (not reacting with H_2) deposited on the Ni surface.

Since no O_2 was available from the gas phase, the only possible explanation is the release of oxygen from the YSZ support, at these high temperatures, which readily reacts with graphitic carbon toward CO formation. CO formation (ca. 250 ppm) was detected during CH_4 decomposition on Ni/SiO_2 and Ni/H-ZSM-5 [10]. Its origin was attributed to the oxidation of the carbon species by residual hydroxyl species on the supporting material [10].

It is known from the literature that YSZ releases oxygen at temperatures above 800 K, thus being transformed into nonstoichiometric oxide [37,38]. Zafeiratos and Kennou [41] showed that Ni nanoparticles interfaced with YSZ single crystal are oxidized into NiO at temperatures above 700 K due to the mobility and spillover of O originating from the YSZ. In a recent article Tsiplakides and Vayenas [42] have measured for the first time the absolute potential of electrodes interfaced with YSZ and they concluded that the absolute voltage of the electrode is determined by the $O^{\delta-}$ double layer which is formed because of the spillover of O^{2-} from the YSZ substrate/solid electrolyte all over the electrode surface at temperatures higher than 600 K.

However in the case of catalyst 2 the presence of small quantities of Mo 1% wt seems to affect significantly the development and reactivity of graphitic layers. As shown in Fig. 10 H_2 reacts with carbon species toward CH_4 even at temperatures exceeding 900 K without any CO formation. It is worth noting that these species are formed at temperatures corresponding to region III of Fig. 9 where the carbon activity α_c is very close to 1, implying that the chemical potential of these carbon species is very close to that of graphitic carbon. Such behavior reveals the positive effect of small quantities of Mo on the inhibition of adsorbed graphitic layer formation. Borowiecki et al. [43] studied the effect of Mo as a promoter on the activity and resistivity to coke of Ni supported on Al_2O_3 during the carbon deposition and gasification reactions under steam reforming and dehydrogenation of *n*-butane. They concluded that Mo itself does not exhibit any specific effect on the rate of carbon deposition during the hydrogenolysis of *n*-butane. However the promoting role of a small Mo addition is quite evident in the presence of H_2O or H_2 as the gasification agents of the carbon deposits. Similarly in the present study the thermodynamic behavior of CH_4 dissociation (Fig. 9) indicates that the surface species on both catalysts 1 and 2 are similar as the two equilibrium curves coincide with each other. However, the difference in hydrogenation activity of the two catalysts (Figs. 4 and 10) can be attributed to the promoting role of Mo in activating H_2 toward the hydrogenation of C_g species into CH_4 [43].

5. Conclusions

The main conclusions of the present study can be summarized as follows:

(i) The equilibrium dissociative adsorption of CH_4 on Ni–YSZ catalysts revealed the formation of three main carbon species as these were detected by reacting with H_2 to produce CH_4 and with O_2 to produce CO_2 and H_2. Carbidic species (C_c) are reactive with H_2 and O_2 at temperatures below 600 K while adsorbed carbon (C_a) species in equilibrium with CH_x species react with H_2 and O_2 above 600 K. Graphitic carbon layers (C_g) are formed upon CH_4 adsorption above 700 K and its main characteristic is the absence of any reactivity with H_2 to form CH_4.

(ii) The binding energy of C_a species with respect to graphite decreases with increasing coverage ranging between 7.32 ± 0.03 and 6.5 ± 0.04 eV for the low (< 0.2 ML) and high (≈ 1 ML) coverage, respectively.

(iii) The presence of 1% wt of Mo either suppresses the formation of nonreacting adsorbed graphitic layers or enhances the reactivity of H_2 toward CH_4 at temperatures higher than 800 K. This behavior reveals the positive effect of Mo in inhibiting the formation of adsorbed graphitic layers.

Acknowledgment

This work was supported by the INCO2-COPERNICUS2 programme of the European Commission under contract ICA2-CT-2000-10003.

References

[1] A.L. Lee, R.F. Zabransky, W.J. Huber, Ind. Eng. Chem. Res. 29 (1990) 766.
[2] S. Bebelis, A. Zeritis, C. Tiropani, S.G. Neophytides, Ind. Eng. Chem. Res. 39 (2000) 4920.
[3] I.V. Yentekakis, Y. Jiang, S.G. Neophytides, S. Bebelis, C.G. Vayenas, Ionics 1 (1995) 491.

[4] M. Stoukides, Catal. Rev. Sci. Eng. 42 (2000) 1.
[5] T. Horita, N. Sakai, T. Kawada, H. Yokokawa, M. Dokiya, J. Electrochem. Soc. 143 (1996) 1161.
[6] G.L. Semin, V.D. Belyaev, V.A. Sobyanin, Appl. Catal. A 181 (1999) 131.
[7] I. Alstrup, T. Tavares, J. Catal. 135 (1992) 147.
[8] I. Alstrup, T. Tavares, J. Catal. 139 (1993) 513.
[9] R.T. Baker, I.S. Metcalfe, Ind. Eng. Chem. Res. 34 (1995) 1558.
[10] T.V. Choudhary, C. Sivadinarayana, C.C. Chusuei, A. Klinghoffer, D.W. Goodman, J. Catal. 199 (2001) 9.
[11] V. Ponec, Catal. Rev. Sci. Eng. 18 (1978) 151.
[12] D.W. Goodman, R.D. Kelley, T.E. Madey, J.T. Yates Jr., J. Catal. 63 (1980) 226.
[13] R.M. Watwe, H.S. Bengaard, J.R. Rostrup-Nielsen, J.A. Dumesic, J.K. Nørskov, J. Catal. 189 (2000) 16.
[14] R.W. Joyner, G.R. Darling, J.B. Pendry, Surf. Sci. 205 (1988) 513.
[15] J.R. Rostrup-Nielsen, in: J.R. Anderson, M. Boudart (Eds.), Catalysis Science and Technology, Vol. 5, Springer, Berlin, 1983, p. 3.
[16] C.-T. Au, M.-S. Liao, C.-F. Ng, J. Phys. Chem. 102 (1998) 3959.
[17] C. Elmasides, D.I. Kondarides, S.G. Neophytides, X.E. Verykios, J. Catal. 198 (2001) 195.
[18] L. Isett, J.M. Blakely, Surf. Sci. 58 (1976) 397.
[19] M. Eizenberg, J.M. Blakely, Surf. Sci. 82 (1979) 228.
[20] J. Galuszka, J.R. Chang, Y. Amenomiya, J. Catal. 68 (1981) 172.
[21] A. Takeuchi, H. Wise, J. Phys. Chem. 87 (1983) 5372.
[22] Q.Y. Yang, K.J. Maynard, A.D. Johnson, S.T. Ceyer, J. Phys. Chem. 102 (15) (1995) 7735.
[23] H. Nakano, S. Kawakami, T. Fujitani, J. Nakamura, Surf. Sci. 454–456 (2000) 259.
[24] A. Barbier, E.B. Pereira, G. Martin, Catal. Lett. 45 (1997) 221.
[25] D.J. Klinke II, W. Steffen, L.J. Broadbelt, J. Catal. 178 (1998) 540.
[26] A. de Koster, R.A. van Santen, J. Catal. 127 (1991) 141.
[27] H. Burghgraef, A.P.J. Jansen, R.A. van Santen, Surf. Sci. 324 (1995) 345.
[28] G.R. Darling, J.B. Pendry, R.W. Joyner, Surf. Sci. 221 (1989) 69.
[29] K. Jacobsen, J.K. Nørskov, Surf. Sci. 166 (1986) 539.
[30] T. Borowiecki, A. Golebiowski, Catal. Lett. 25 (1994) 309.
[31] T. Borowiecki, A. Golebiowski, B. Stasinska, Appl. Catal. A 153 (1997) 141.
[32] J.-S. Choi, K.-I. Moon, Y.G. Kim, J.S. Lee, C.-H. Kim, D.L. Trimm, Catal. Lett. 52 (1998) 43.
[33] J. Laine, J. Brito, F. Severino, Appl. Catal. 15 (1985) 333.
[34] I. Chen, F.-L. Chen, in: C.H. Bartholomew, J.B. Butt (Eds.), Catalyst Deactivation, Elsevier, Amsterdam, 1991, p. 253.
[35] H.P. Klug, L.E. Alexander, in: X-Ray Diffraction Procedures, 2nd ed., Wiley, New York, 1974, p. 642.
[36] B. Hammer, J.K. Nørskov, Adv. Catal. 45 (2000) 71.
[37] J. Xue, R. Dieckmann, in: T.A. Ramanarayanan, W.L. Worrell, H.L. Tuller (Eds.), Proc. of the 2nd Int. Symp. on Ionic and Mixed Ceramics, Vol. 94-12, The Electrochemical Society, Pennington, NJ, 1994, p. 191.
[38] R. Dieckmann, J. Phys. Chem. Solids 59 (4) (1998) 507.
[39] N. Triantafyllopoulos, S.G. Neophytides, in preparation.
[40] G.G. Tibbetts, J. Crystal Growth 66 (1984) 632.
[41] S. Zafeiratos, S. Kenou, Surf. Sci. (2002), in press.
[42] D. Tsiplakides, C.G. Vayenas, Surf. Sci. 467 (2000) 23.
[43] T. Borowiecki, G. Giecko, M. Panczyk, Appl. Catal. A: Gen. 230 (2002) 85.